WILEY ONLINE LIBRARY
Early View publication on
www.wileyonlinelibrary.com
(issue and page numbers not yet assigned;
citable using Digital Object Identifier – **DOI**)

J. Biophotonics 1–14 (2012) / **DOI** 10.1002/jbio.201200091

Journal of
BIOPHOTONICS

FULL ARTICLE

Correlation of temperature rise and optical coherence tomography characteristics in patient retinal photocoagulation

Stefan Koinzer[*,1], *Kerstin Schlott*[2], *Lea Portz*[1], *Lars Ptaszynski*[3], *Alexander Baade*[3], *Marco Bever*[3], *Mark Saeger*[1], *Amke Caliebe*[4], *Renè Denner*[5], *Reginald Birngruber*[3], *Ralf Brinkmann*[2,3], *and Johann Roider*[1]

[1] Dept. of Ophthalmology, University of Kiel, House 25, Arnold-Heller-Str. 3, 24105 Kiel, Germany
[2] Institute of Biomedical Optics, University of Lübeck, Peter-Monnik-Weg 4, 23562 Lübeck, Germany
[3] Medical Laser Center Lübeck GmbH, Peter-Monnik-Weg 4, 23562 Lübeck, Germany
[4] Institute of Medical Informatics and Statistics, University of Kiel, House 31, Arnold-Heller-Str. 3, 24105 Kiel, Germany
[5] Carl Zeiss Meditec AG, Göschwitzer Str. 51–52, 07745 Jena, Germany

Received 16 May 2012, revised 3 July 2012, accepted 8 July 2012
Published online 16 August 2012

Key words: laser photocoagulation, optoacoustics, photocoagulation, retinal temperature, spectral domain optical coherence tomography, OCT, subthreshold, classification

Supporting information for this article is available free of charge under http://dx.doi.org/10.1002/jbio.201200091

We conducted a study to correlate the retinal temperature rise during photocoagulation to the afterward detected tissue effect in optical coherence tomography (OCT). 504 photocoagulation lesions were examined in 20 patients. The retinal temperature increase was determined in real-time during treatment based on thermoelastic tissue expansion which was probed by repetitively applied ns laser pulses. The tissue effect was examined on fundus images and OCT images of individualized lesions. We discerned seven characteristic morphological OCT lesion classes. Their validity was confirmed by increasing visibility and diameters. Mean peak temperatures at the end of irradiation ranged from approx. 60 °C to beyond 100 °C, depending on burn intensity.

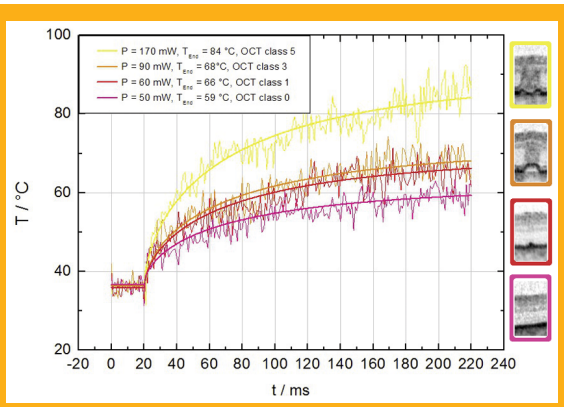

The abstract figure shows temperature profiles and corresponding OCT images of selected 300 µm, 200 ms photocoagulation lesions.

* Corresponding author: e-mail: Koinzer@auge.uni-kiel.de, Phone ++49 (4 31) 5 97–46 97, Fax ++49 (4 31) 5 97–24 28

Journal of BIOPHOTONICS

1. Introduction

Since its introduction in the 1940s [1], photocoagulation has become and remained the standard therapy for various retinal diseases, particularly ischemic retinal conditions [2]. Its therapeutic effect is caused by a light-induced temperature increase in the retinal pigment epithelium (RPE), which spreads to adjacent retinal layers and causes tissue coagulation. Since this temperature increase is unknown during clinical treatment, laser dosage is based on the immediate ophthalmoscopical effect of previous lesions. Factors that vary from one location to the next such as light transmission and pigmentation have a strong influence on the effect but cannot be prospectively incorporated in laser power adjustment. Hence, only monitoring of the retinal temperature rise during application of each photocoagulation lesion would allow adjustment of its individual effect.

During the past three decades, experimental retinal temperature measurements have been attempted by thermoprobes [3, 4] by magnetic resonance imaging [5] or by high-speed infrared thermoimaging [6]. None of these methods is feasible during clinical photocoagulation treatment. Theoretical models to determine retinal temperatures [7, 8] allow estimation of average threshold temperatures in a set of photocoagulation lesions, but they do not allow prediction of the temperature course in an individual lesion due to the unknown optical properties of the particular eye and treatment location. Different attempts to automate laser power control based on measurement of modulated light reflection were not applicable in clinical practise [9–11].

Non-invasive determination of the temperature rise during retinal laser treatment has been achieved by optoacoustics. Its initial applications were selective retina therapy (SRT) by Schuele et al. [12] and transpupillary thermo therapy by Kandulla et al. [13]. Our group has recently modified this method for retinal photocoagulation [14, 16]. Nanosecond laser pulses were simultaneously and collinearly applied with the treatment irradiation. These repetitive pulses excited thermo-elastic pressure transients from the irradiated tissue, which were detected on the ocular surface by a transducer in the laser contact lens and allowed calculation of the retinal temperature profile over time. The measured signals have been shown to facilitate automatic, prospective treatment laser control in animals in order to achieve homogenous lesions independently of local tissue variation [14, 16].

In order to apply automatically temperature-controlled photocoagulation clinically, first the knowledge of the therapeutically desired temperature rise is required. Theoretical and basic studies have been conducted by others in order to determine retinal pigment epithelium (RPE) cell viability threshold temperatures and retinal rupture threshold temperatures [6, 8, 15]. Temperatures necessary to induce specific burn intensities, however, have never been systematically determined. It is the intention of the present study to characterize photocoagulation lesions by spectral-domain optical coherence tomography (SD-OCT) and correlate their temperature measurements to characteristic SD-OCT appearances. The findings provide temperature endpoints for patient photocoagulation.

2. Material and methods

2.1 Laser device and retinal temperature measurement

A standard photocoagulator (VISULAS VITE, Carl Zeiss Meditec AG) was modified for temperature measurements. The laser emits repetitive nanosecond laser pulses simultaneously and collinearly to the treatment radiation. By the pulses it excites thermo-elastic pressure waves at the coagulation site. Wave amplitudes depend on the retinal temperature, since the thermo-elastic tissue expansion coefficient depends on the temperature [12, 13, 16]. The pressure waves travel through the eye and are detected with an annular ultrasonic transducer, which is embedded in a standard laser contact lens (Mainster focal grid lens, modified by the Medical Laser Center Luebeck GmbH). A cable conducts the signals through an amplifier and via a D/A processing card (CompuScope 8347, Gage Applied Technologies) into a personal computer. The complete setup is shown in Figure 1. Additionally, the computer receives a trigger signal from the photocoagulator if a photocoagulation has been effected by the physician. The optoacoustic pressure rise is converted to retinal temperature rise by software. The entire pressure detecting and processing unit was manufactured by the Medical Laser Center Luebeck GmbH and certified to fulfil CE requirements. Details of the theory and technical background of optoacoustic measurements has been published elsewhere [16].

For calibration purposes, optoacoustic pulse recording starts 20 ms prior to the continuous wave (CW) treatment laser. The optoacoutic response to these calibration signals is assigned the relative value of 100%, and it corresponds to the actual retinal temperature, which equals body temperature. All consecutive optoacoustic transients, that are received from the lesion, are normalized to these calibration pulses. The resulting relative optoacoustic amplitudes can be converted to temperatures by the knowledge of the tissue expansion coefficients [16]. Some representative temperature curves of different lesions are given in Figure 2. In order to compensate for pressure fluctuations and noise, the data course was best fitted

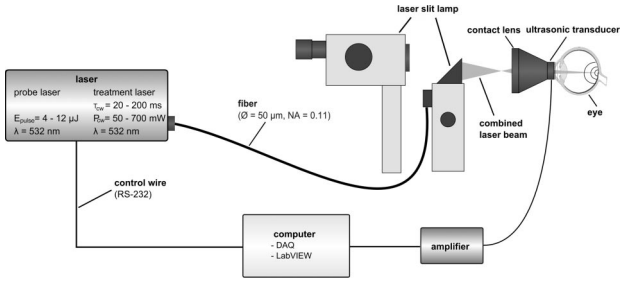

Figure 1 Schematic illustration of the experimental setup. A laser source emits pulsed probe irradiation at a repetition rate of 1 kHz and simultaneously continuous wave (cw) treatment irradiation (both Nd:YAG, $\lambda = 532$ nm). Irradiation is transmitted via a standard laser slit lamp and contact lens system. The probe pulses induce temperature-dependent acoustic pressure waves from the fundus, which can be detected on the ocular surface. The optoacoustic signals are amplified and digitized by a fast computer oscilloscope card. A real-time LabVIEW® routine analyzes the signals during photocoagulation.

to the theoretically expected temperature course, which was determined by adequate solution of the heat diffusion equation as described elsewhere, e.g. by Roider and Birngruber [8, 18]. The raw data are plotted by thin lines and the fit functions by thick lines in Figure 2a, while b shows only fit functions of a set of photocoagulation lesions.

Optoacoustics determine a mean temperature response of the irradiated tissue volume. In the case of photocoagulation, the temperature value of interest is the spatial temperature peak which occurs in the center of the spot at the RPE. By solution of the heat diffusion equation, the peak temperature can be calculated from the mean temperature. The temperature values specified in this study indicate the temporal and spatial maximum at the end of the exposure in the center of the lesion at the RPE. These values were calculated from the fit function of each lesion as described above. Details are given by Brinkmann et al. [16].

For treatment, probe pulse energies (4, 8, 12 µJ) and pulse repetition frequencies (500 Hz, 1 kHz) could be chosen. We used 4 µJ pulses for 100 µm lesions and 12 µJ pulses for 300 µm lesions, all at a repetition rate of 1 kHz. Apart from that, treatment was performed like any routine therapy.

2.2 *Clinical study*

Laser lesions were examined in a non-interventional, prospective clinical study on 20 patients receiving photocoagulation for diabetic retinopathy (16/20), diabetic maculopathy (4/20), retinal vein occlusion (3/20) or occlusive vasculitis (1/20). The study was reviewed and approved by the institutional ethics committee at Kiel University (application no. A 105/10) and was carried out in accordance with the contents of the declaration of Helsinki. All treatment in-

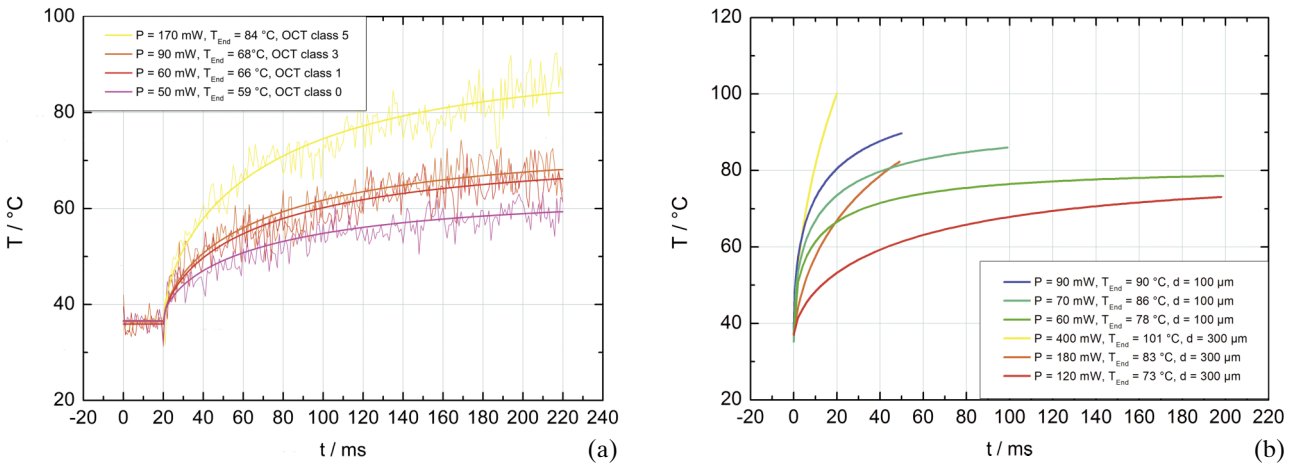

Figure 2 (online color at: www.biophotonics-journal.org) Representative optoacoustically measured temperature data over time. (**a**) shows selected 300 µm, 200 ms lesions of OCT classes 0, 1, 3 and 5 (from bottom to top). Thin lines represent optoacoustic raw data, while thick lines show best fits to the theoretically expected temperature profiles. The fit functions were used to calculate end temperatures. The end temperatures increase with increasing OCT class. Treatment laser powers, peak end temperatures and achieved OCT classes are indicated for each lesion. (**b**) shows exemplary fit functions of irradiations that achieved very similar OCT class 3 or 4 lesions, either in 100 µm irradiations (blue/green lines) or in 300 µm irradiations (yellow/red lines) and by different irradiation times. The end temperatures of lesions with common diameters are expected to connect to different Arrhenius functions (not shown). Treatment laser powers, peak end temperatures and irradiation diameters are indicated for each lesion.

dications followed the treatment guidelines of the German ophthalmological society that were valid at the time of treatment [19, 20]. All treatments were performed by the the same physician (SK).

Before the laser treatment began, we chose an appropriate study area of retina outside the temporal vessel arcades or nasally to the optic disc (Figure 3a). The study area was imaged by color fundus images (Zeiss FF450 plus fundus camera, Carl Zeiss Meditec AG, Jena, Germany), infrared images and SD-OCT images (HRA + OCT Spectralis®, Heidelberg Engineering, Heidelberg, Germany) before the treatment and at timepoints 1 hour, 1 week (day 5–8) and 1 month (day 22–30) after treatment.

An OCT image of $15 \times 20°$ determined the size of the study area. Before the treatment started, we scanned the selected area in 30 µm steps. Every sectional image was obtained by averaging of 20 sweeps to optimize image quality. All study lesions were placed within the area that had been previously scanned by OCT (Figure 3b). Using the follow-up function (AutoRescan™), we imaged identical section planes in all consecutive examinations. Once a lesion could be identified in any one of the examinations, we traced it backward and forward through the whole series of OCT images.

We performed routine laser treatment for diabetic maculopathy (100 µm, 100 ms, faint whitening lesions) and diabetic retinopathy (300 µm, 200 ms, moderate whitening lesions) on 4 patients and evaluated a subset of the lesions in our study. In the remaining 16 patients, we varied lesion parameters systematically. We used spot diameters of 100 or 300 µm and exposure times of 20, 50, 100 or 200 ms for exposure times. Threshold powers of ophthalmoscopical visibility were titrated outside the study area. In the study area, we applied rows of five lesions, starting at threshold power and increasing power lesionwise in step widths as provided by the laser device (50–200 mW: 10 mW-steps, 200–500 mW: 20 mW-steps, >500 mW: 50 mW-steps). In other rows of lesions, power was decreased from the threshold in the same manner (Figure 3a). Each patient received 20–50 study lesions, depending on the diameter of the lesions, in order to assure sufficient treatment in the study area. Outside the study area, patients received routine photocoagulation therapy according to the guidelines cited above.

During the treatment, laser lesions were mapped in a printed fundus image by the treating physician. Having aquired the 1 hour follow up images, we inscribed the spot identifications into a digital follow up image (Figure 3a). Where necessary, OCT images were consulted in order to allocate the lesions correctly. Infrared and OCT follow up images after 1 week and 1 month were also used to cross-check lesion locations (Figure 3b).

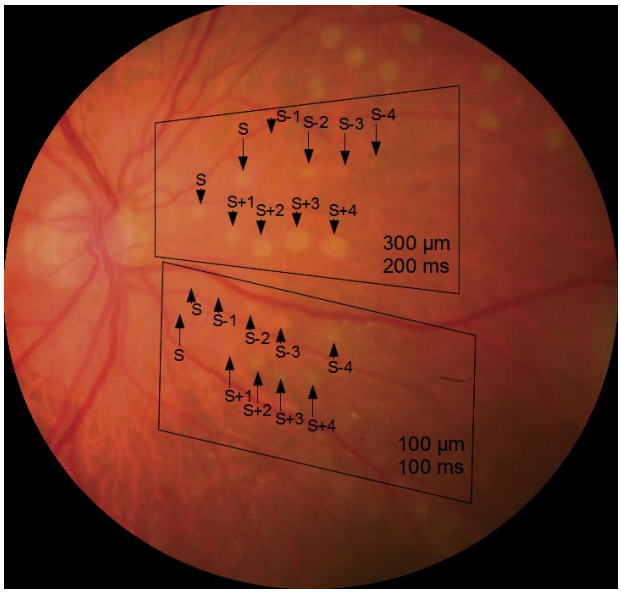

(a)

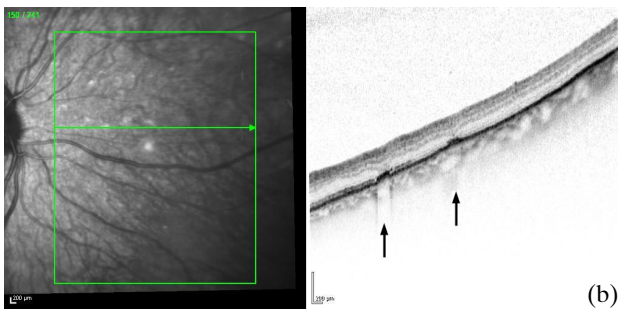

(b)

Figure 3 (online color at: www.biophotonics-journal.org) (**a**) shows a representative mapped fundus color image of a study area. 4 rows of study lesions of either 300 µm, 200 ms or 100 µm, 100 ms were applied. Power was chosen to increase from the threshold of immediate clinical visibility (S . . . S+4) or to decrease from the threshold of immediate clinical visiblity (S . . . S-4). Arrows indicate the position of each lesion as confirmed by OCT analysis. (**b**) shows an OCT image of the corresponding fundus after 7 days as delivered by the OCT machine. The green arrow in the infrared image on the left indicates the section plane. Laser lesions that are cut in the cross sectional image on the right are 300 µm, 200 ms S+2 (left arrow) and S+4 (right arrow). Note that the scale of the sectional image is 4 times larger in vertical than in horizontal direction.

2.3 Ophthalmoscopical lesion size measurements

Lesion diameters were assessed on the digital color fundus images taken 1 hour after the end of the treatment. In order to measure the size of a lesion, it was contoured manually in an image editing software (Gimp 2). All marked lesions' pixel sizes were semi-automatically measured by ImageJ software,

and the pixel and real diameters calculated. The scaling factor for the pixel-to-μm calculation was retrieved from the camera manufacturer's software and was 4.385 μm per pixel (50° photographs).

Every lesion was measured by three independent observers. A lesion was considered visible if at least two observers recognized it, and the mean diameter was used for evaluation. If one of three values deviated much from the other two (standard deviation $>= 40$ μm, and median value not in the middle of extreme values), it was excluded from the evaluation.

Photocoagulation lesions show a whitish-grey zone of denaturation on the fundus, which develops over 10 minutes after the irradiation. Intense burns have an additional bright white core of thermal necrosis, which occurs immediately after the irradiation. Both were included in the diameter measurement. An additional halo of edema, which may develop around intense burns over hours, however, was considered a secondary effect and excluded from the measurements.

2.4 Qualitative OCT classification

All lesions that could be identified in OCT were digitally cut out and mounted in a composite of 4 consecutive images (pre-treatment, 1 hour, 1 week, 1 month post). These composites were arranged in groups of lesions with common diameter – exposure-time settings, giving the following 7 groups: For *100 μm diameter*, 20 ms, 50 ms, 100 ms and 200 ms exposure times (4 groups) and for *300 μm diameter*, 20 ms, 50 ms and 200 ms exposure times (3 groups). Within each group, we looked for common attributes of the lesions and arranged them in subgroups with apparently increasing intensity. This led to 7 consecutive classes of OCT morphologies. The numbers of lesions that were observed in every class, depending on exposure time and irradiation diameter, are given in Table 2 (supporting information online).

2.5 OCT lesion size measurements

The greatest linear diameter (GLD) of a lesion was measured in the OCT software. Measurements were carried out in the 1μm : 1μm depiction, which we scaled up to 800% magnification. We measured the lesion size at the photoreceptor inner segments (IS), or, in class 2 lesions, at the outer nuclear layer (ONL).

2.6 Statistics

The association of two categorical variables was tested by Fisher's exact test. Continuous variables were assumed to be normally distributed, and association with factors was tested via analysis of variance with and without interaction between factors and also for strata of the factors. Model selection was performed by backward selection. Association between two continuous variables was investigated by linear regression analysis.

P-values below 0.05 were considered significant. In cases of multiple testing, like in stratified evaluation of laser lesion parameters, *p*-values were adjusted for multiple testing by the Bonferoni method. All statistical analyses were carried out with the statistical software R, version 2.10.1 [21].

3. Results

OCT classes (Figure 4)

Illustrations and examples of OCT classes are given for 300 μm lesions in Figure 4a and for 100 μm lesions in Figure 4b, respectively. With respect to slightly variable appearance of the OCT classes, two different illustrations are shown for classes 3 and 5. During development of the classification, the different appearances of these classes had been thought to represent different entities. However, similiarities during wound healing, their neighboring occurrence within groups of lesions with similar power and their temperature values lead to the conclusion, that these OCT groups must represent identical burn intensities of variable appearance. Except for class 1 lesions, we classified all lesions in OCT images taken one hour after treatment.

Lesions that never became visible in OCT were classified subthreshold, class 0. Those that were invisible after one hour, but would show small dense particles close to the RPE later on, were graded class 1. As soon as any retinal lesion was apparent after one hour, lesions were graded class 2. The first layer where changes became visible was the ONL. In class 2 lesions, the photoreceptor inner segment – outer segment (IS-OS) junction line and OS were intact. Stronger lesions showed a broad column of signal increase in the ONL, an interruption of the IS-OS junction and changes in the OS layer as well, but normal thickness of the RPE/BM-complex. These were graded class 3. A sub-RPE bleb was facultative in class 3 and was more likely to occur in longer/larger exposures. If the RPE/BM complex underneath a lesion was thinned and the RPE at the lesion border was elevated as small warts, the lesion was graded class 4. They occurred exclusively in short exposure lesions. Class 5 lesions had thin, but attached RPE in the lesion center, but were surrounded by a ring of detached (long exposure) or excavated (short exposure) RPE. The strongest type of lesion that we

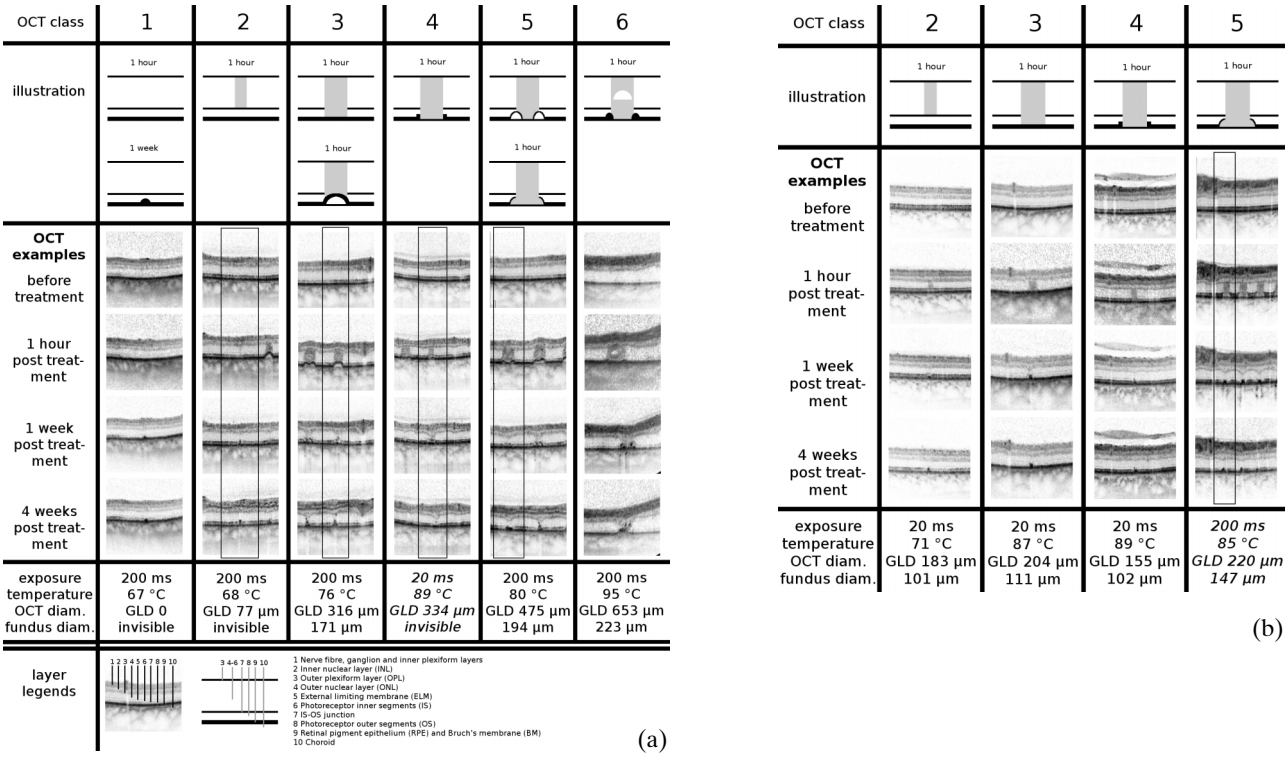

Figure 4 (**a**) and (**b**) show the characteristic lesion appearance of each lesion class as determined in this study. (**a**) displays examples of 300 µm lesions at 200 ms exposure time. Since class 4 lesions did not occur at 200 ms exposure time, a 20 ms lesion is displayed instead. (**b**) displays examples of 100 µm lesions at 20 ms exposure time. Since class 5 lesions did not occur at 20 ms exposure time, a 200 ms lesion is displayed for this particular class. Class 1 and class 6 lesions were rarely or not at all achieved in 100 µm irradiations and are not shown.
Illustrations of each class are shown on top of the columns, and below representative OCT images taken before treatment and 1 hour, 1 week and 1 month after the treatment. All images in a column show the same fundus lesion during follow up. At the bottom line, the exposure time, peak temperature, greatest linear diameter (GLD) as measured in OCT and the diameter as measured on the fundus color image are given. All diameter measurements and lesion classification were made at images taken 1 hour after treatment with the exception of class 1 lesions, that were not detectable after 1 hour. If an OCT image shows more than one lesion, a black box demarcates the lesion of interest. The legends of OCT and illustration layering and layer abbreviations are given in (**a**) below.
A detailed description of characteristic signs for each OCT class is given in the text.
Note that the same peak temperature will produce different burn intensities at different exposure times (e.g. Figure 4a, class 4, and b, class 5).

observed, class 6, showed the typical column of signal increase in the ONL like classes 3–5, but had a bright spot in the center of this column.

The qualitative OCT analysis of consecutive lesions classes after 1 week and 1 month showed that the amount of retinal damage, which includes axial and horizontal extension of OCT alteration, increases with increasing classes. A quantitative analysis of OCT GLD's showed that GLD's decrease over the first month, and that the decrease is more pronounced in hotter or higher class lesions. The strongest decrease was about ¼ of the initial GLD. Class 1 lesions had, per definition, increasing GLD's, because their GLD after one hour was zero. 300 µm, class 2 lesions showed slightly growing GLD's as well.

Ophthalmoscopic visibility (Figure 5)

The percentage of lesions that were detectable in 1 hour color fundus images is depicted for each lesion class in Figure 5. The differences between OCT classes are highly significant as determined by Fisher's exact test ($p < 0.001$), while the influences of exposure time ($p = 0.08$) and irradiation diameter ($p = 0.43$) are not significant. For better consistency with other results, rates of visibility are displayed for 100 µm (light gray bars) and 300 µm lesions (dark gray bars) separately in spite of statistical insignificance, but the overall evaluation (white bars) is also shown and the number of observations in each group as well.

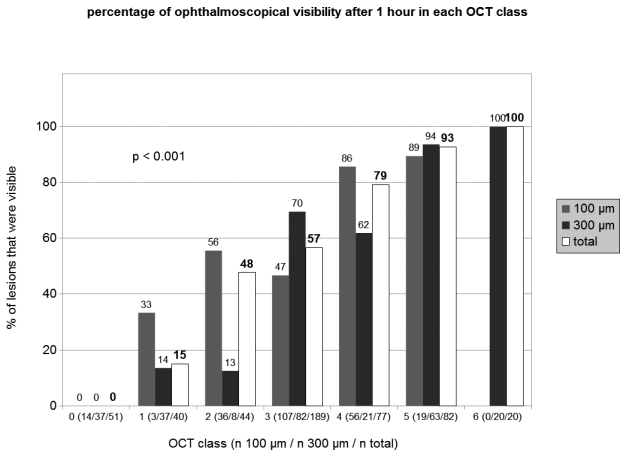

Figure 5 Displays the percentage of lesions in each OCT class that were visible on color fundus images one hour after treatment. The total number of lesions that occurred in each class is indicated in brackets next to the class label. Considering a delay until retinal blanching fully develops, lesions up to class 3 are unlikely to be visible during treatment (see also Table 1).

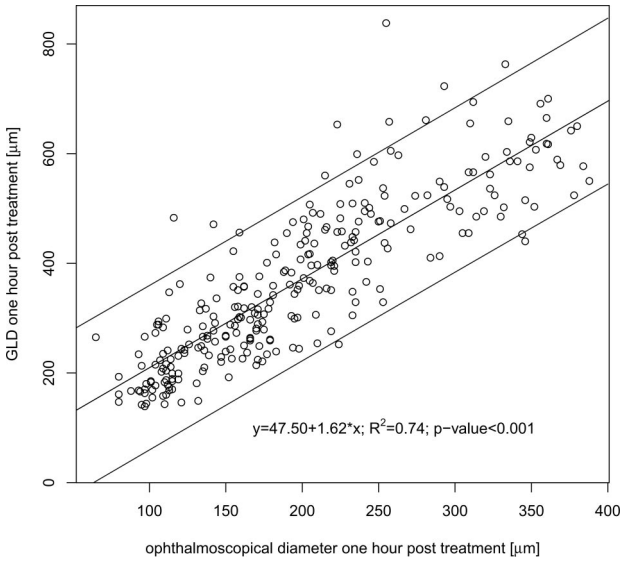

Figure 6 Linear regression analysis of lesion diameters as assessed by OCT cross sectional images (greatest linear diameter, GLD) and by color fundus image measurement. All measurements were obtained one hour after treatment. Sub-threshold lesions that were not detected in either OCT or color fundus images were excluded from the regression analysis.

Class 0 lesions were per definition invisible. Among 40 class 1 lesions, only 15% were visible, with a high degree of imprecision in the small subgroup of class 1, 100 µm lesions (1/3 visible). 100 µm lesions have a tendency to become visible sooner than 300 µm lesions (e.g. 56% vs. 13% for class 2). There is an obvious and significant increase of visibility rates with increasing OCT classes. Note that the rates of visibility were determined in 1 hour fundus images and do not represent immediate visibility rates during treatment.

Correlation of ophthalmoscopical diameter and OCT GLD (Figure 6)

Only lesions that were detectable both on fundus images and in OCT sectional images were included in the linear regression analysis. There is good linear correlation of ophthalmoscopical lesions diameters with OCT GLD ($R^2 = 0.74$, $p < 0.001$). Conse-

Table 1 Properties of clinical endpoint photocoagulation lesions, measured during routine macular and panretinal photocoagulation for diabetic maculopathy and retinopathy in 4 patients. Due to changes of optoacoustic properties in denaturating tissue, true peak temperatures during panretinal treatment are most likely higher than calculated in Table 1.

	300 µm, 200 ms **macular treatment**	300 µm, 200 ms **panretinal treatment**
OCT class 3 (n/%)	12/34%	3/5%
OCT class 4 (n/%)	23/66%	3/5%
OCT class 5 (n/%)	–	34/59%
OCT class 6 (n/%)	–	18/31%
sum (n/%)	*35/100%*	*58/100%*
ophthalmoscopically invisible (n/%)	6/17%	1/2%
peak end temperature [°C] (mean ± standard deviation)	100 ± 23	90 ± 17
ophthalmoscopical diameter [µm] (mean ± standard deviation)	151 ± 77	312 ± 62
OCT GLD [µm] (mean ± standard deviation)	255 ± 40	536 ± 84

quently, statements concerning OCT GLD's of different lesion classes are also qualitatively applicable for ophthalmoscopical diameters (Figures 7 and 8). The linear equation ($y = 47.5 + 1.62 \cdot x$) indicates that lesions are 1.5 to 2 times larger in OCT measurements than in color fundus images.

Stratified correlation of OCT GLD's and OCT classes (Figure 7)

Only lesions with OCT GLD's > 0 one hour after treatment were evaluated in this correlation. Consequently, OCT classes 0 and 1 were excluded. There was a significant dependency of GLD over OCT class ($p < 0.001$), over irradiation diameter ($p < 0.001$) and over exposure time ($p < 0.001$). The statistical interactions of OCT class and irradiation diameter, of OCT class and exposure time and of irradiation diameter and exposure time were all highly significant ($p < 0.001$). Therefore, data in Figure 7 are given for all strata separately. Identical statistical evaluation of ophthalmoscopic lesion diameters over OCT classes was also done and gave similar results (data not shown). We chose to display GLD results because there are fewer sub-threshold lesions than in fundus image assessment.

In 100 µm lesions (Figure 7a), GLD's increase significantly as the exposure time increases in class 3 and 4 lesions (both $p > 0.001$), but not in class 2 lesions ($p = 0.13$). In class 2, the GLD is about twice the spot size. In class 3 and 4 lesions, the GLD ranges from almost twice the spot size (20 ms) to about 4 times the spot size (200 ms). GLD's increase slightly but significantly as OCT classes increase for 50 and 100 ms lesions ($p = 0.02$ and $p = 0.007$), but not for 20 and 200 ms lesions ($p = 1$).

In 300 µm lesions (Figure 7b), GLD's increase with increasing exposure time in class 4 and 5 lesions ($p = 0.03$ and p 0.01), but not in class 2 and 3 lesions ($p = 1$ and $p = 0.23$). GLD's are smaller than the irradiated spot in class 2, equal to the irradiated diameter in class 3 and range from 125% (20 ms) to 180% (200 ms) the spot size in classes 4 to 6. GLD's increase with increasing OCT classes for 50 and 200 ms lesions (both $p < 0.001$), but not for 20 ms lesions ($p = 0.11$).

Stratified evaluation of lesion temperatures (Figure 8)

Average peak end temperatures of stratified OCT classes are displayed for 100 µm lesions (Figure 8a) and 300 µm lesions (Figure 8b). The data in Figure 8 are depicted analogous to Figure 7. Subthreshold (class 0) lesions were excluded from average temperature evaluation. Optoacoustic temperature meas-

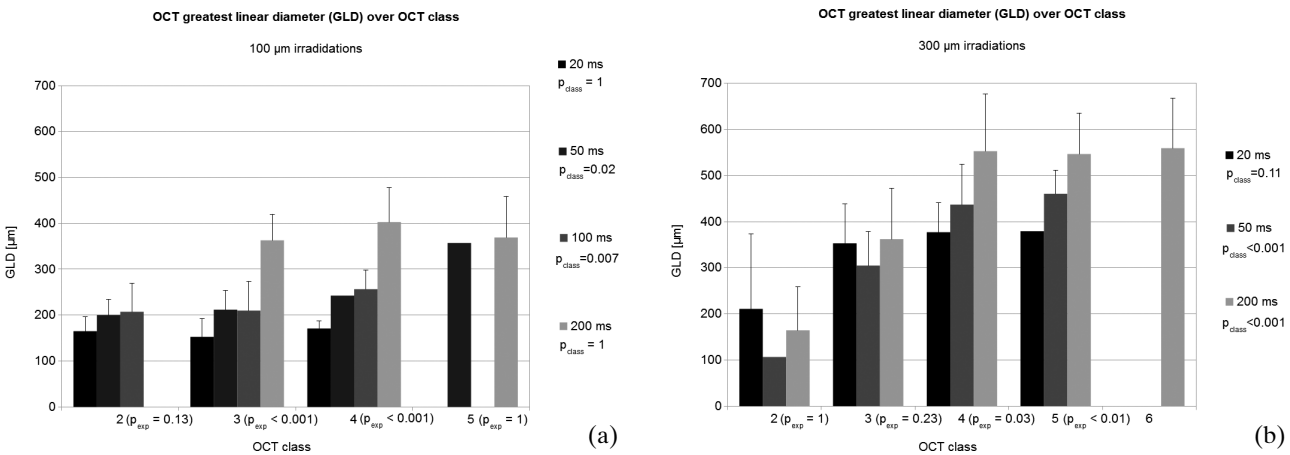

Figure 7 Mean OCT greatest linear diameters (GLD's, 1 hour after treatment) over OCT classes, stratified for different exposure times and irradiation diameters (**a**: 100 µm; **b**: 300 µm). Standard deviations are indicated by error bars for each group with at least 3 observations. The influence of OCT class ($p < 0.001$), irradiation diameter ($p < 0.001$) and exposure time ($p < 0.001$) on the GLD is highly significant. The statistical interactions of OCT class and irradiation diameter, of OCT class and exposure time and of irradiation diameter and exposure time were also highly significant ($p < 0.001$). Only lesions with OCT GLD's > 0 one hour after treatment were included; consequently, OCT classes 0 and 1 were excluded from the analysis.
p_{exp}: *P*-values for differences in GLD between different exposure times for a fixed OCT class.
p_{class}: *P*-values for differences in GLD between different classes for a fixed exposure time.
Shown *p*-values are adjusted for multiple testing according to Bonferoni's method ($n = 4$ tests for all strata except exposure time strata in 300 µm: $n = 3$ tests).

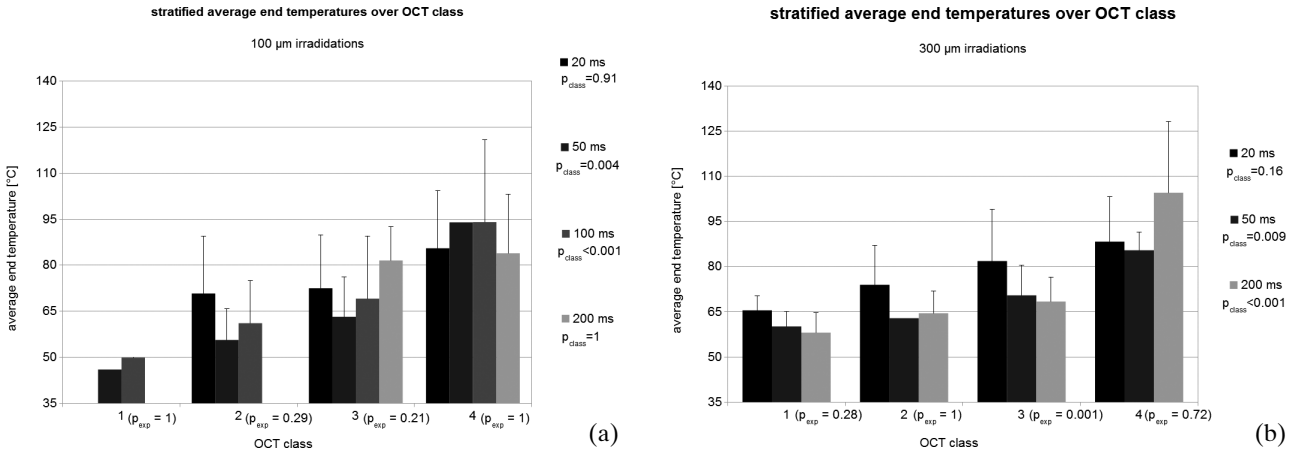

Figure 8 Average peak end temperatures over OCT classes, stratified for different exposure times and irradiation diameters (**a**: 100 µm; **b**: 300 µm). Standard deviations are indicated by error bars for each group with at least 3 observations. The influence of OCT class ($p < 0.001$), irradiation diameter ($p = 0.009$) and exposure time ($p < 0.001$) on the GLD is highly significant. The statistical interactions of OCT class and irradiation diameter, of OCT class and exposure time and of irradiation diameter and exposure time were not significant ($p > 0.05$). End temperature calculations of strong coagulations (class 5 and 6) yield false low values. Consequently, only OCT classes 1–4 are displayed.
p_{exp}: *P*-values for differences in average peak temperature between different exposure times for a fixed OCT class.
p_{class}: *P*-values for differences in average peak temperature between different classes for a fixed exposure time.
Shown *p*-values are adjusted for multiple testing according to Bonferoni's method ($n = 4$ tests for all strata except exposure time strata in 300 µm: $n = 3$ tests).

urements of lesion classes 5 and 6 were also excluded because they yield erroneously low values (see discussion below).

There was a significant dependency of temperature over OCT class ($p < 0.001$), over irradiation diameter ($p = 0.009$) and over exposure time ($p = 0.001$).

None of the pairwise interactions of the influence factors was significant ($p > 0.05$). In the 100 µm group, only 3/236 lesions achieved class 1, and temperature data are of little significance.

In the 300 µm, class 3 group, average temperatures were 81.8 ± 17 °C at 20 ms, 70.5 ± 10 °C for 50 ms and 68.4 ± 8 °C for 200 ms ($p = 0.001$). Here, temperatures that achieved identical OCT classes decreased as exposure times increased, as can be expected from the thermal damage model of Arrhenius (7). In all other groups, the average temperatures did not differ significantly. Increasing OCT classes correspond to increasing temperatures. For example, in the 300 µm, 50 ms group, average temperatures were 60.1 ± 5 °C in class 1, 63 °C in class 2, 70.5 ± 10 °C in class 3 and 85.4 ± 6 °C in class 4 lesions. Temperatures occurring at identical exposure times and identical OCT classes were higher in 300 µm than in 100 µm irradiations, with one exception: In 100 µm lesions, the highest OCT class (4) had higher average temperatures than in 300 µm lesions. Obviously, further temperature increases did not change the OCT appearance in 100 µm lesions, but in 300 µm lesions where class 5 and 6 morphologies occurred.

In summary, average peak temperatures of class 1 lesions were around 60 °C, of class 2 lesions around 65 °C, of class 3 lesions around 70 °C and of class 4 lesions around 85 to 90 °C, depending on lesion diameter and exposure time.

Characteristics of clinical endpoint photocoagulation lesions (Table 1)

Macular lesion power was adjusted to achieve barely visible spots during treatment (100 µm, 100 ms). These lesions achieved classes 3 (34%) and 4 (66%). 17% of lesions were invisible in 1 hour fundus images. Classes 1 and 2 were not achieved at all in 35 lesions. Lesion diameters were 151 ± 77 µm ophthalmoscopically and 255 ± 40 µm in OCT, which is 151% and 255% of the irradiation laser beam diameter, respectively. The average peak end temperature was 100 ± 23 °C.

ETDRS panretinal lesion power was adjusted to achieve moderate retinal blanching, but no necrotic bright lesion center (300 µm, 200 ms). These exposures achieved few class 3 and 4 lesions (5% each), but predominantly class 5 (59%) and 6 (31%) lesions. 98% of 58 panretinal lesions were visible after 1 hour. Lesion diameters were 312 ± 62 µm ophthalmoscopically and 536 ± 84 µm in OCT, which is 104% and 179% of the irradiation laser beam diameter, respectively. Average peak temperatures were 90 ± 17 °C.

4. Discussion

This study gives a systematic analysis of OCT morphologies and retinal temperatures in 532 nm photocoagulation lesions. The analysis includes clinically important variations of lesion diameters (100/300 μm), exposure times (20/50/100/200 ms) and laser powers. Moreover, we included an analysis of standard lesions in order to correlate our findings to clinical standard lesions. We used 100 μm, 100 ms for macular treatment and 300 μm, 200 ms for ETDRS panretinal treatment. Besides the 100 μm, 100 ms and 300 μm, 200 ms parameter combinations, 20 ms lesions of both diameters have also become increasingly important since the introduction of pattern laser photocoagulation [22, 23].

We evaluated 35 lesions in the 100 μm, 100 ms and 58 lesions in the 300 μm, 200 ms routine treatment groups, respectively. Additionally, our study design included at least 50 lesions of every diameter-exposure combination in the patients with systematic parameter variation, but 101 lesions of the 300 μm, 200 ms setting. The latter gave the most accurate temperature results and the finest modulation of OCT morphologies and was thus most promising to allow specific conclusions. Moreover, this parameter set is of great importance for panretinal photocoagulation, which accounts for the majority of retinal photocoagulations.

This study intends to correlate laser lesion temperatures to the tissue damage intensity of different supra-threshold burn classes, where supra-threshold means biologically effective as visible in OCT. An objective characterisation of photocoagulation lesions is difficult. Different threshold criteria such as RPE cell survival, angiographic or clinical lesion visibility have been used in basic research and to examine sub-threshold photocoagulation [6, 8, 15, 18, 24]. Clinicians widely use 3–4 step grading scales of ophthalmoscopic whitening (25–27), that suffer from significant inter-observer variation and are time-dependent. Instead of funduscopic grading, we evaluated lesion visibility (for threshold lesions) and diameters (for supra-threshold lesions) in fundus color images after one hour. These parameters are readily available during treatment, and were correlated to SD-OCT findings, for which no standardized evaluation has been established so far. We found that fundus diameters correlate linearly to OCT GLD's, but are smaller by a factor of 1.5 to 2 according to the linear equation given in Figure 6. Hence, the conclusions we draw concerning OCT GLD's apply qualitatively to fundus diameters as well.

Muqit et al. examined 392 μm, 20–200 ms lesions in OCT and found GLD's to be smaller than the irradiation diameter in mild coagulations [19], which agrees with our findings (300 μm, class 2 lesions). For stronger coagulations, GLD's increased to 100% (20 ms) and up to 125% (200 ms) in Muqit's study. The corresponding (mean) values were 125% (20 ms) and 180% (200 ms) in our study. The differences may be due to different OCT devices used and to an observer-dependency of GLD evaluation. Interestingly, the ratio of GLD and irradiation diameter was larger in 100 μm irradiations (153–403 μm, or 1.53–4.03 fold, and 2.55 fold in clinical endpoint treatment) than in 300 μm irradiations (211–559 μm, or 0.70–1.86 fold, and 1.79 fold in clinical endpoint treatment). Although 100 μm lesions are generally considered safer for macular coagulation, our findings indicate that the safety margin around a lesion should be kept wider in 100 μm than in 300 μm irradiations. Possibly, the final lesion size after successive growth during the scarring process is related to the comparably large intial OCT lesion size.

Since the availability of histological data from human material is limited, SD-OCT has been applied in a number of studies to examine tissue effects of photocoagulation [25, 29, 30]. Muqit et al. examined systematically varied supra-threshold green laser lesions, and Mojana et al. examined subthreshold to soft infrared lesions [31, 32]. A comprehensive OCT study that compared sub-threshold to mETDRS lesion intensities of a broad range of lesion parameter variations has not been conducted to our knowledge. While the aforementioned studies used single scan SD-OCT devices, we conducted repetitive SD-OCT scanning of identical retinal planes, averaging 20 scans per sectional image which gives more detailed insight into ultra structural tissue alterations by improved image quality. Nevertheless, the qualitative and quantitative appearance of photocoagulation lesions differs significantly in OCT images and in histology (own, unpublished analysis). Comparing the histological lesion diameter to the ophthalmoscopical diameter, Jain et al. found the histological lesion to be greater by 15% in 10 ms lesions and decreasing until it was smaller by 30% in 100 ms lesions [28]. Obviously, with regard to the ophthalmoscopical diameter, histological and OCT diameters are inversely correlated. Therefore, an OCT classifier for human lesions cannot be deduced from findings in (animal) histology.

Our OCT analysis led to seven consecutive lesion classes as displayed in Figure 4, some of which have already been observed by others [31, 32], while some classes were newly described in our study due to either improved image resolution, to increased parameter variation or to a different treatment wave length. In accordance with the cited studies, OCT alterations of the inner retinal layers were only rarely detected. Coagulation particularly of the ganglion and nerve fiber layer (GL) should be avoided, since it is thought to cause extended scotoma. Histological analyses show that the GL is indeed affected by coagulations of common intensity, even at powers

slightly above the threshold of ophthalmoscopic visibility [14]. In contrast, our OCT images even of intense 100 μm lesions did not show any affection of the ONL or beyond, and 300 μm lesions showed inner layer affection only in single, very intense burns. Obviously, OCT underestimates significantly the impact of photocoagulation on the inner retinal layers. Thus, in spite of its great clinical importance and histologically proven occurrence in rabbits, inner layer damage as detected in OCT is not considered in our lesion classification. The validity of our OCT classes and of their order is supported by increasing damages after 1 week and 1 month (Figure 4), by an increasing percentage of visibility (Figure 5), by increasing GLD's and increasing funduscopical diameters (Figure 7) and by increasing temperatures (Figure 8).

As expected, the frequencies of OCT classes varied between the different diameter-exposure time groups (Table 2, supporting information online). Some morphologies appear more likely in specific parameter groups, like class 4 that only occurred in 20/50 ms exposures or class 6 that only occurred in 300 μm/200 ms exposures. Some combinations did not occur at all or only rarely, like class 1 in 100 μm, 20 ms lesions. In these cases a statistical analysis is not possible. On the other hand, we achieved subthreshold, class 0, lesions in all groups except for 100 μm, 200 ms. Consequently, our OCT analysis should include the softest possible and continuously increasing lesion intensities up to, but not beyond ETDRS standard intensity. Consequently, we cannot display retinal ruptures or choroidal bleedings in our analysis, and we cannot exclude that lesion morphologies exist between our class 6 and retinal rupture.

Our photocoagulator was a prototype that allowed simultaneous temperature assessment during treatment. The device was easily compatible with everyday requirements for clinical routine, which distinguishes it from other methods of temperature measurement during photocoagulation [3–6]. Calculation of absolute retinal temperatures was possible after the patient's body temperature had been determined [16]. The system allowed 1000 temperature measurements per second, which is fast enough to monitor even short photocoagulation exposures of 20 ms. The optoacoustic probe laser grants temperature measurement exactly at the site of treatment and at the depth of actual laser light absorption.

The accuracy of temperature measurements was determined to be $\pm$ 15% ΔT, where ΔT depicts the temperature rise from body temperature [33]. In general, the accuracy of optoacoustic measurement is higher for longer exposures due to an increased number of single measurements, and for larger irradiations. The latter allow to use higher pulse energies without inducing RPE evaporation, and thus facilitate an improved signal-to-noise ratio. The optoacoustic measurement relies on signal calibration to the actual treatment site, which is done over 20 ms before the CW laser starts. If the optoacoustic tissue properties change, for example during strong coagulations, the signal calibration becomes invalid. Then, the optoacoustic signal amplitudes decrease and falsely indicate falling tissue temperatures, which begins at temperatures around 95 °C. For higher temperatures, we assume that our measurements are lower than the real value.

Laboratory investigations tend to determine retinal temperatures at biologically critical thresholds like RPE cell death. RPE viability could not be determined in our study, but it is reasonable to assume that the RPE is lethally impaired in class one lesions. These show small dense particles in OCT follow up images, which supposedly represent an RPE healing reaction. In 300 μm, class 1 lesions, we measured average end temperatures of 65.4 °C for 20 ms, 60.0 °C for 50 ms and 58.1 °C for 200 ms exposures. Denton et al. determined 53 °C to be the threshold temperature for retinal cell death at various laser exposure times (100, 250 and 100 ms [6]). Based on an Arrhenius model, Sramek et al. postulated threshold temperatures for RPE cell viability to be 63 °C at 20 ms, 60 °C at 50 ms, 56 °C at 100 ms and 53 °C at 200 ms in 50 μm-lesions, while the threshold temperature for retinal rupture was 180 °C [8]. Particularly Sramek's data correspond very well to our measurements (Figure 8).

The systematic temperature analysis in Figure 8 reveals that for classes 1 and 2, end temperatures are around 65 °C for 20 ms exposures and around 60° for longer exposures. These classes are ophthalmoscopically invisible, because barely visible macular lesions (100 μm, 100 ms) achieved higher OCT classes (3 and 4). However, classes 1 and 2 do show a long-term OCT effect, and are therefore biologically effective. Consequently, the temperature endpoint of biologically active, but ophthalmoscopically invisible photocoagulation should be around 60–65 °C, depending on exposure time. OCT classes 3 and 4 were predominantly achieved in barely visible macular treatments and corresponded to temperature measurements of 70 to 90 °C. Thus 80–85 °C seems appropriate for mild photocoagulation and corresponds to the mean temperature measurement of 90 °C in macular routine treatment. Moderate lesions that are intended in panretinal ETDRS treatments were achieved at a (mean) measured temperature of 100 °C, which must be assumed to be determined too low as discussed above. Due to this measurement error, the corresponding OCT classes 5 and 6 were excluded from the evaluation in Figure 8. Since none of the lesion groups up to class 4 achieved higher temperatures than 95°C, a temperature endpoint of 95–100 °C can be expected to be appropriate for panretinal treatment.

Temperature endpoints of 65 °C for sub-threshold, of 80 °C for mild macular and of 95 °C for panretinal photocoagulation differ sufficiently to be discriminated by the optoacoustic measurement, the accuracy of which is expected around ± 15% ΔT (corresponding to ±9 °C at 97 °C). Even if the error bars in Figure 8 show significant overlap, the temperature variations between different OCT classes are statistically significant for 100 µm, 50 and 100 ms groups and for 300 µm, 50 and 200 ms groups. Statistically significant temperature variation within one OCT class, but for different exposure times, was only found in 300 µm, class 3 lesions. The exposure-time correlates to temperatures as predicted by the Arrhenius theory [7]. To determine these correlations more exactly for all different parameter groups and OCT classes, further research will be necessary that might either improve temperature measurement accuracy or increase statistical power in a larger cohort.

On the other hand, our study has revealed significant inaccuracy of routine laser dosage. Particularly panretinal lesions produced OCT classes 3 to 6. Moreover, the analysis of ophthalmoscopical visibility showed, that lesions of any OCT class may become visible. Obviously, clinical visibility gives a clue on the likelihood to achieve a certain tissue morphology, but it has significant uncertainty. Hence, temperature controlled photocoagulation but not conventional laser control has the potential to reliably produce a desired ultrastructural tissue effect.

5. Conclusions

Optoacoustic temperature measurement during photocoagulation is applicable on patients. It allows for the first time the assessment of the retinal temperature profile in real time at each individual spot during delivery of routine photocoagulation. The temperature data correspond well to consecutive classes of OCT-morphological retinal damage. The optoacoustic data are useful to implicate automatic, temperature-feedback controlled photocoagulation for mild supra-threshold lesions, which has already been applied successfully in rabbits [14, 17].

Conflict of interests R. Brinkmann holds patent rights. R. Denner is employed by Carl Zeiss Meditec (patent rights).

Acknowledgements This collaborative project is supported by the German Ministry of Education and Research (BMBF) according to the Innovation Award for Advancing Medical Technology 2006, grant #01EZ0734 (Dept. of Ophthalmology, Kiel University), #01EZ0732 (Medical Laser Center Lübeck), #01EZ0733 (Institute of Biomedical Optics Lübeck) and #01EZ0735 (Carl Zeiss Meditec AG).

Stefan Koinzer graduated with an M.D. at the University of Kiel, Germany, in 2004. He did his internship in Offenburg, Germany, and at the University of Kiel, Germany, and completed his specialty training in ophthalmology in 2009. Since 2009 he has been working as a research fellow between the Medical Laser Center Luebeck and the Dept. of Ophthalmology at the University of Kiel. Besides retinal laser photocoagulation control, his research focusses on ocular histopathology and RPE.

Kerstin Schlott received a M.Sci. degree in physics from the University of Hamburg in 2007. She is currently working on a Ph.D. in the optoacoustic research group of the Institute of Biomedical Optics at the University of Luebeck. Her research interests are the optoacoustic temperature determination during retinal photocoagulation, the development of an automatic coagulation control and the effect of the fundus tissue's optical parameters on the temperature distribution during laser irradiation.

Lea Portz has received medical training at the Universities of Göttingen, Germany, and Kiel, Germany, and expects to graduate with an M.D. in 2013. She has been part of the collaborative laser photocoagulation group as part of her scientific training since early 2011, with a methodological focus on clinical evaluation of photocoagulation lesions in high-resolution spectral-domain OCT. Her research interests include medical retina.

Lars Ptaszynski received his diploma in engineering from the University of Applied Sciences in Luebeck, Germany, in 2007. Then he joined Ralf Brinkmann's group at the Medical Laser Center in Luebeck and worked in the field of laser photocoagulation, with a focus on mild and subthreshold laser device control and automation. Since 2012, he has been employed by Opmedt GmbH, Luebeck, Germany, working on OCT development.

Alexander Baade received a M.Sci. degree in physics from the Johannes Gutenberg University of Mainz, Germany, in 2009, with a specialization in quantum optics. In the same year he joined Ralf Brinkmann's group at the Medical Laser Center Luebeck for a Ph.D. project. His research topics comprise investigations on the accuracy of noninvasive realtime temperature determination during retinal photocoagulation, relevant numerical simulations and tissue optics.

Marco Bever received a M.Sci. degree in physics from the University of Hamburg, where his special interests were laser physics and irradiation biology. He received a Ph.D. in 2011 at the Institute of Biomedical Optics at the University of Luebeck. From 2008 to 2012, he worked on a post doc scientist position in the colla-

borative optoacoustics photocoagulation control group at the Medical Laser Center Luebeck. Since 2012, he has been employed by Philips Healthcare, Hamburg, Germany.

Mark Saeger graduated with an M.D. at the University of Kiel, Germany, in 2005. He did his internship at the Dept. of Ophthalmology, University of Kiel, Germany, and completed his specialty training in ophthalmology in 2011. He has been working as a clinician-scientist since then, and his scientific interests are retinal photocoagulation, corneal infectious diseases and others.

Amke Caliebe is a mathematician and received a Ph.D. in 1999 at the University of Kiel, Germany. Since 2003, she has held a permanent research, consulting, and teaching position at the Institute for Medical Statistics at the University of Kiel. Her research interests include population genetics, statistical genetics and statistical forensics. She has been cooperating with the Institute of Clinical Molecular Biology, Kiel, with a focus on genetic epidemiology and the genetics of healthy ageing.

Renè Denner received his diploma in engineering from the University of Applied Sciences, Jena, Germany, in 2005. Since then, he has been working for Carl Zeiss Meditec AG with a focus on photocoagulation laser development. He has been part of the collaborative research group on optoacoustic photocoagulation control since 2007 and contributed to the project by implementation of prototype patient laser devices.

Reginald Birngruber has been a professor for medical biophysics at the University of Luebeck, Germany, since 1992. From 1992 to 2010, he was CEO and research director of the Medical Laser Center Luebeck, and from 2005 to 2010 he was the director of the Institute of Biomedical Optics at the University of Luebeck. Reginald Birngruber held teaching positions at the University of Munich, Germany, at Harvard University, Boston, MA, and at the Massachusetts Institute of Technology (MIT).

Ralf Brinkmann is a physicist and holds a Ph.D. from the University of Luebeck, Germany. He is CEO of the Medical Laser Center Luebeck and affiliated with the Institute of Biomedical Optics at the University of Luebeck. His main R&D fields cover therapeutic lasers with a focus on minimally invasive IR laser surgery and ophthalmic laser applications. With respect to ophthalmology, refractive surgery, selective retina therapy and feedback controlled retinal photocoagulation are worth mentioning.

Johann Roider graduated with an M.D. from the University of Munich, Germany in 1989. He worked as research fellow and clinical scientist at the Wellman laboratories of Photomedicine, Boston, and at the Universities of Lübeck and Regensburg. Since 2002 he has been the chairman of the Dept. of Ophtalmology at the University of Kiel. His research interests are laser-tissue interactions, pathogenesis and molecular targets in age related macular degeneration, and new applications in vitreoretinal surgery.

Literature

[1] G. Meyer-Schwickerath and Albrecht Von Graefes, Arch. Ophthalmol. **156**, 2–34 (1954).
[2] A. M. Shah, N. M. Bressler, and L. M. Jampol, Am. J. Ophthalmol. **152**, 332–339 (2011).
[3] R. Birngruber, in: Laser Applications in Medicine and Biology, M. Wolbarsht (ed.), (New York: Plenum Press, 1991), pp. 277–357.
[4] L. M. Parver, C. R. Auker, and D. O. Carpenter, Retina **2**, 117–20 (1982).
[5] S. Maswadi, S. Dodd, J. Gao, and R. Glickman, J. Biomed. Opt. **9**, 711–718 (2004).
[6] M. L. Denton, G. D. Noojin, M. S. Foltz, C. D. Clark 3rd, L. E. Estlack, B. A. Rockwell, and J. R. Thomas, J Biomed Opt. **16**, 036003 (2011).
[7] R. Birngruber, F. Hillenkamp, and V. P. Gabel, Health Phys. **48**, 781–796 (1985).
[8] C. Sramek, Y. Paulus, H. Nomoto, P. Huie, J. Brown, and D. Palanker, J Biomed Opt. **14**, 034007 (2009).
[9] O. Pomerantzeff, G. J. Wang, M. Pankratov, and J. Schneider, Arch. Ophthalmol. **101**, 949–953 (1983).
[10] M. R. Jerath, R. Chundru, S. F. Barrett, H. G. Rylander 3rd, and A. J. Welch, Arch. Ophthalmol. **111**, 531–534 (1993).
[11] J. Inderfurth, R. Ferguson, M. Frish, and R. Birngruber, Lasers Surg. Med. **15**, 54–61 (1994).
[12] G. Schuele, H. Elsner, C. Framme, J. Roider, R. Birngruber, and R. Brinkmann, J. Biomed. Opt. **10**, 64022 (2005).
[13] J. Kandulla, H. Elsner, R. Birngruber, and R. Brinkmann, J Biomed Opt. **11**, 041111 (2006).
[14] S. Koinzer, K. Schlott, L. Ptaszynski, M. Bever, S. Kleemann, M. Saeger, A. Baade, A. Caliebe, Y. Miura, R. Birngruber, R. Brinkmann, and J. Roider, Invest. Ophthalmol. Vis. Sci. **53**, 3605–3614 (2012).
[15] C. Framme, A. Walter, P. Prahs, D. Theisen-Kunde, and R. Brinkmann, Lasers Surg Med. **40**, 616–624 (2008).
[16] R. Brinkmann, S. Koinzer, K. Schlott, L. Ptaszynski, M. Bever, A. Baade, S. Luft, Y. Miura, J. Roider, and R. Birngruber, J. Biomed. Opt. **17**, 061219 (2012).
[17] K. Schlott, S. Koinzer, L. Ptaszynski, M. Bever, A. Baade, J. Roinder, R. Birngruber, and R. Brinkmann, J. Biomed. Opt. **17**, 061223 (2012).
[18] J. Roider, F. Hillenkamp, T. Flotte, and R. Birngruber, Proc. Natl. Acad. Sci. U.S.A. **90**, 8643–8647 (1993).
[19] [Statement of the German Ophthalmological Society, the Retinological Society and the Professional Asso-

ciation of German Ophthalmologists on Therapy for Macular Oedema in Cases of Retinal Vein Occlusion], Klin Monbl Augenheilkd. **227**, 542–556 (2010).
[20] [Recommendation of the Retinological Society, the German Ophthalmological Society and the Professional Association of Ophthalmologists in Germany: treatment of diabetic maculopathy], Klin Monbl Augenheilkd. **228**, 446–459 (2011).
[21] R. Foundation for Statistical Computing, Vienna, Austria (2009), available at: http://www.R-project.org.
[22] R. Velez-Montoya, J. L. Guerrero-Naranjo, C. C. Gonzalez-Mijares, J. Fromow-Guerra, G. R. Marcellino, H. Quiroz-Mercado, and V. Morales-Cantón, Br. J. Ophthalmol. **94**, 720–724 (2010).
[23] M. M. K. Muqit, G. R. Marcellino, J. C. B. Gray, R. McLauchlan, D. B. Henson, L. B. Young, N. Patton, S. J. Charles, G. S. Turner, and P. E. Stanga, Br. J. Ophthalmol. **94**, 1493–1498 (2010).
[24] J. Roider, N. A. Michaud, T. J. Flotte, and R. Birngruber, Arch. Ophthalmol. **110**, 1786–1792 (1992).
[25] H. Kang, L. Su, H. Zhang, X. Li, L. Zhang, and F. Tian, Graefes Arch. Clin. Exp. Ophthalmol. **248**, 1705–1711 (2010).
[26] M. O. Tso, I. H. Wallow, and S. Elgin, Arch. Ophthalmol. **95**, 1035–1040 (1977).
[27] Y. M. Paulus, A. Jain, R. F. Gariano, B. V. Stanzel, M. Marmor, M. S. Blumenkranz, and D. Palanker, Invest. Ophthalmol. Vis. Sci. **49**, 5540–5545 (2008).
[28] A. Jain, M. S. Blumenkranz, Y. Paulus, M. W. Wiltberger, D. E. Andersen, P. Huie, and D. Palanker, Arch. Ophthalmol. **126**, 78–85 (2008).
[29] M. Bolz, K. Kriechbaum, C. Simader, G. Deak, J. Lammer, C. Treu, C. Scholda, C. Prünte, and U. Schmidt-Erfurt, Ophthalmology **117**, 538–544 (2010).
[30] M. M. K. Muqit, J. C. B. Gray, G. R. Marcellino, D. B. Henson, L. B. Young, N. Patton, S. Charles, G. Turner, A. Dick, and P. Stanga, Arch. Ophthalmol. **128**, 448–455 (2010).
[31] M. M. K. Muqit, J. Denniss, V. Nourrit, G. R. Marcellino, D. B. Henson, I. Schiessl, and P. Stanga, Invest. Ophthalmol. Vis. Sci. **52**, 994–1002 (2011).
[32] F. Mojana, M. Brar, L. Cheng, D. U.-G. Bartsch, and W. R. Freeman, Retina **31**, 235–242 (2011).
[33] A. Baade, K. Schlott, S. Luft, L. Ptaszynski, M. Bever, R. Birngruber, and Ralf Brinkmann, Proc. SPIE **8092**, 80921B (2011).

